Romanian Journal of Petroleum & Gas Technology
VOL. V (LXXVI) • No. 2/2024

ANALYSIS OF FRACTURE GEOMETRY IN FLUID DRAINAGE AFTER HYDRAULIC FRACTURING. CASE OF WINK MS-09 IN MAKELEKESE FIELD, D.R. CONGO

Rachidi Opuluku [1,2*]

Joel Etshekodi Lohadje [1,3]

Olivier Kimpesa Dyese [1]

Gracias Kingombe Manianga [1]

Jean Iyolo Lungembo [1]

Dirk Akili Bihivu [1]

[1] University of Kinshasa, Faculty of Petroleum, Gas and New Energies, D.R. Congo
[2] Centre for geological and mining research, D.R. Congo
[3] National Geological Service of Congo, D.R. Congo
* e-mail (corresponding author): rachidiopuluku1@gmail.com

DOI: 10.51865/JPGT.2024.02.02

ABSTRACT

In this paper, we analyze stimulation by hydraulic fracturing with the aim of establishing a relationship between fracture geometry and hydrocarbon drainage. Believes fracturing geometry is an effective means of predicting the productive capacity of a hydrocarbon reservoir and the productivity of a well stimulated by hydraulic fracturing is closely linked to the fracturing geometry. Demonstrate the impact of fracturing geometry on the productivity of a hydrocarbon reservoir. Characterize the different parameters of the fracturing geometry while determining the link between these parameters; highlight the difference between the productivity of the reservoir before and after fracturing and monitor the evolution of productivity in relation to this geometry.

Keywords: Makelekese oilfield, fracture geometry, hydraulic fracturing, well productivity, hydrocarbon drainage

INTRODUCTION

The purpose of subjecting an oil or gas reservoir to hydraulic fracturing is to allow the oil or gas to drain more easily between the medium that contains it and the wellbore: this process is known as stimulation. Almost all the North American coastal reservoirs that remain today require, to some extent, to be stimulated in this way in order to achieve a profitable production rate. [1]

Indeed, in order to write this work properly, we asked ourselves a few guiding questions, which are as follows:

- ✓ What impact does fracturing geometry have on the drainage of hydrocarbons around the well?
- ✓ Can fracturing geometry predict the production capacity of an oil reservoir?
- ✓ Is there a link between fracturing geometry and the productivity of an oil well?

Our answer to these questions is that fracturing geometry is an important element to monitor when treating a well by hydraulic fracturing, as it has a very strong influence on the drainage of hydrocarbons around the well.

The paper represents a study on the impact of fracture geometry on the hydrocarbon drainage in the Cenomanian reservoir of the Makelekese field, located in the coastal basin of the Republic of Congo. The study focuses on three fractured horizons (I, H and G) and analyses the evolution of hydrocarbon productivity as a function of fracture geometry. The study makes a significant contribution to understanding the relationship between fracture geometry and hydrocarbon drainage in low-permeability reservoirs. The results of the study will enable oil operators to optimise the design of hydraulic fracturing operations in order to improve the profitability of hydrocarbon deposits.

This study highlights the crucial relationship between fracture geometry and reservoir productivity. From a scientific point of view, this research has made some major contributions, including:

- An innovative approach to hydraulic fracturing: The study focuses on the influence of fracture geometry on hydrocarbon drainage, offering a novel perspective in this field;
- Significant impact of fracture geometry: The results show that fracture geometry plays a decisive role in hydrocarbon productivity, particularly in low-permeability reservoirs;
- Recommendations for oil operators: The study suggests that operators focus on fracturing geometry during future exploitation campaigns, thereby optimizing hydrocarbon production.

The study recommends extending the research to other fracturing models and different types of reservoir in order to establish a more general compatibility relationship between fracture geometry and reservoir performance. In summary, this study makes a valuable contribution to understanding the optimisation of hydraulic fracturing operations to improve hydrocarbon production in low-permeability reservoirs.

MATERIALS AND METHODS

Our research used data from the PERENCO-REP company, followed by bibliographic consultation in our libraries and digital consultation on the internet, then data processing using ArcGis 10, Grapher 8 and Microsoft pack software.

The coastal basin of the Democratic Republic of Congo is located in the province of Central Congo, precisely in the town of Muanda, and lies between 12°00' and 12°45' East longitude and 5°30' and 6°00' South latitude. It is 42km wide and covers an area of 5,992 square kilometres. it is about 600km from the city of Kinshasa. Figure 1 below shows the location of the field under study.

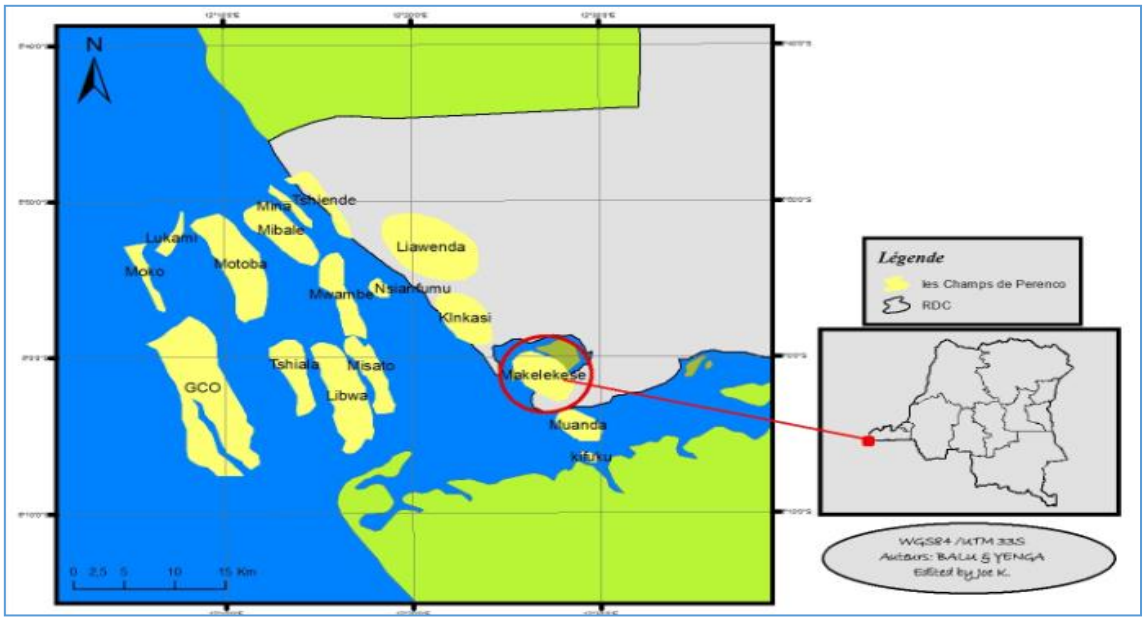

Figure 1. *Map of DRC offshore oil fields* [13]

In the Democratic Republic of Congo, the different sedimentation zones that give surface and source rock indices are the central basin (non-productive basin), the eastern part of the Democratic Republic of the Congo or the grabens of lakes Albert, Edouard, Kivu, Tanganika, Mwero and others (non-productive basins), the West Congo basin which extends from Gabon to Namibia (non-productive basin) and the coastal or littoral zone (productive). [2].

PETROPHYSICAL PROPERTIES OF THE CENOMANIAN RESERVOIR OF THE MAKELEKESE FIELD

The study of the petrophysical properties and fluid flows of rocks requires knowledge and understanding of the nature of the microstructure and microgeometry of the rocks. [3]. This study is essential in particular to describe an oil reservoir, the functioning of an aquifer or to predict the importance of fluid movements in a volcanic edifice or around a waste storage site. [4]

- ✓ **Porosity**

Porosity is a petrophysical property characterizing a certain fluid storage capacity in a tank. This is an essential property to control during production because if rocks are compressible in a deposit, they are subject to geostatic pressure and the pressure of the fluids present in the pores; when the latter decreases as a result of production, the rock compresses until a new equilibrium is reached.

The porosity of a reservoir is directly related to its geological history (diagenetic) and depends on the size of the grains, their shape, their classification or arrangement as well as the distribution of pores throughout the reservoir. [5, 6]

It should be remembered that the porosity that occurs in the deposits is that which allows the circulation of fluids in the pores; it is the useful porosity that corresponds to the pores connected to each other with the outside. [7].

- ✓ **Permeability**

During mining, fluids circulate in rock pores with varying degrees of ease, depending on the characteristics of the porous medium. The intrinsic or absolute permeability of a rock is the ability of this rock to allow a fluid to circulate through its pores, of which it is saturated. It can be quantified by Darcy's law, an experimental law. [8, 9].

The permeability of a rock depends on the connection of the pores, which is a function of many factors including grain size, grain distribution, grading, reservoir heterogeneity, and other factors such as capillary strength that depend on the wettability of the rock. [10].

- ✓ **Saturation**

It is essential to know the nature of the fluids that occupy the pores of the rock. The saturation of a rock sample into a fluid is the ratio of the volume of that fluid in the sample to the volume of Vp pores in the sample. [8].

The Makelekese field is a small field with a complex lithology and multiple reservoirs:

- The Turonian reservoir – this reservoir is made up of clays, carbonated silts and argillaceous carbonates. This reservoir has a net to gross of 100%, porosity of 21% and saturation of 60%. The structure of the field shows that the Turonian of the Makelekese field is gas-bearing. Our study will therefore focus more on the Cenomanian, which contains exploitable liquid hydrocarbons [11, 12].
- The Cenomanian reservoir – this reservoir is defined by a faulted anticline. Unlike the northern fields, here we observe relatively rapid facies changes [11]. Lithologically, the Makelekese Cenomanian is composed of carbonates, silts and clays with a net to gross of 50%, porosity of 15% and saturation of 65%. The thickness of the oil reservoir averages 100 m with an average gas dome boundary of 25 m [11].

The oil-gas contact is observed in zones J and K at a depth of 1011 m and the oil-water contact is observed between zones G and F. The cumulative oil production achieved from the Cenomanian reservoir of the Makelekese field is 3,868,184 barrels (bbls) until 2015. PVT analysis of the Cenomanian reservoir yielded oil at 29°API with a viscosity of 3.96cp, the initial gas-to-oil ratio (GOR) of 257 scf/stb and a formation volume factor of 1.16 res.bbl/stb (Kinkasi data); an initial pressure of 1625 psia at a depth of 1090 m ("MS-8 well") [13].

Hydraulic fracturing is a technique for stimulating a reservoir, which consists of injecting a liquid capable of increasing permeability under pressure into a productive formation or sequence. It is an operation that consists of creating, after the rock has ruptured, a permeable drain extending as far as possible into the formation so as to facilitate the flow to the well. [14, 15, 16, 17, 18].

This fracturing can be carried out close to the surface, or at great depths (more than 1 km, or even more than 4 km in the case of shale gas), and from vertical, inclined or horizontal wells. [18, 19, 20].

✓ **Properties of fracturing fluids**

The choice of the type of hydraulic fracturing fluid is made according to the properties of the reservoir. Although water-based fluids are most commonly used, some reservoirs consist of rock types that contain water-sensitive clays. Other types of fluids are then used. [19].

Water has the advantage of being an inexpensive, easily available and transportable fluid, which does not pose safety problems (fire, explosion, pollution, etc.). Quite easily treatable with additives, its relatively high density makes it possible to limit the pumping power. However, for the same reason, disgorgement can be difficult if the reservoir pressure is low and, on the other hand, the increase in water saturation by filtration reduces the relative permeability of the reservoir. [20, 19, 8].

The common practice in hydraulic fracturing is to start with the penetrating fluids to initiate the fracture and then use the viscous fluid with additives to extend the fracture. The rupture pressure is also a function of the characteristic of the rock and the degree of damage recorded by the formation. [21, 22]

- **Presentation of fracture geometry data**

The fracture geometry data shown in Table 1 below present parameters such as fracture width, length, conductivity and the number of perforations executed in each interval of the Cenomanian reservoir).

***Table 1**: Fracture geometry parameters. (Perenco-Rep, RDC). These data do not show the fracture height, as the fracturing carried out in well MS-09 is horizontal. This is consistent with the radial model. Vertical analysis of fracture geometry parameters [13]*

Zone	*Depth MDm*	*Depth TVDm*	*Fracture width (ft)*	*Fracture length (ft)*	*Conductivity of fractures (MD.ft)*	*Number of perforations*	*Concentration of proppants (Ibm/ft)*
TOP I	*1108*	*1108*	*0*	*0*	*0*	*0*	*0*
I	*1110*	*1110*	*0*	*0*	*0*	*0*	*0*
I	*1112*	*1112*	*0*	*0*	*0*	*0*	*0*
I	*1115*	*1115*	*0.036*	*33.1*	*712*	*26*	*0.32*
I	*1117*	*1117*	*0.046*	*37.9*	*907*	*13*	*0.41*
I	*1118*	*1118*	*0.051*	*38.4*	*1007*	*0*	*0.45*
TOP H	*1119*	*1119*	*0.056*	*41.7*	*1117*	*13*	*0.5*
H	*1120*	*1120*	*0.063*	*48.9*	*1246*	*26*	*0.56*
H	*1122*	*1122*	*0.068*	*52.3*	*1338*	*13*	*0.6*
H	*1123*	*1123*	*0.071*	*53.8*	*1394*	*13*	*0.63*
H	*1124*	*1124*	*0.073*	*54.4*	*1442*	*13*	*0.65*
H	*1125*	*1125*	*0.078*	*56.2*	*1544*	*13*	*0.7*
H	*1126*	*1126*	*0.083*	*57.1*	*1626*	*49*	*0.73*
H	*1127.5*	*1127.5*	*0.095*	*59.2*	*1873*	*16*	*0.85*
TOP G	*1130*	*1130*	*0.106*	*61.7*	*2078*	*66*	*0.94*
G	*1132*	*1132*	*0.11*	*62.3*	*2163*	*13*	*0.98*
G	*1133*	*1133*	*0.113*	*62.3*	*2216*	*26*	*1*
G	*1135*	*1135*	*0.11*	*62.3*	*2155*	*26*	*0.98*

G	*1137*	*1137*	*0.1*	*62.1*	*1968*	*39*	*0.89*
G	*1140*	*1140*	*0.096*	*60.8*	*1894*	*39*	*0.86*
G	*1143*	*1143*	*0.092*	*59.4*	*1801*	*89*	*0.81*
G	*1146*	*1146*	*0.087*	*58.1*	*1705*	*98*	*0.77*
G	*1149*	*1149*	*0.084*	*56.8*	*1649*	*0*	*0.75*
G	*1150*	*1150*	*0.081*	*56.8*	*1590*	*20*	*0.72*
G	*1151*	*1151*	*0.076*	*56.6*	*1499*	*39*	*0.68*
G	*1153*	*1153*	*0.069*	*54.8*	*1360*	*20*	*0.61*
G	*1155*	*1155*	*0.054*	*53.9*	*1058*	*0*	*0.48*
G	*1159*	*1159*	*0.028*	*50.4*	*561*	*0*	*0.25*
G	*1162*	*1162*	*0.015*	*37.4*	*292*	*0*	*0.13*
Bottom	*1167*	*1167*	*0*	*0*	*0*	*0*	*0*

In this work, we use the equivalent of well radius r_w = 0.25 ft.

- **Calculating productivity growth**

Hydraulic fracturing aims to improve the quality of permeability. Having observed the different geometries, it would be useful to understand the productivity resulting from this stimulation operation. We cannot determine fracture productivity without first calculating certain parameters. These are:

✓ **Half-length *Xf***

This is the distance between the well and the point at the end of the fracture along the horizon or sedimentary layer. [23]

$$X_f = \frac{L}{2} \tag{1}$$

✓ **Fracture permeability K_f (mD)** [23]:

$$kf = \frac{F_{CD}}{w} \tag{2}$$

With w: Fracture width, in feet

F_{CD}: the dimensionless Fracture conductivity in mdft

The dimensionless fracture conductivity F_{CD} [23]:

$$F_{CD} = \frac{kf * w}{k * Xf} \tag{3}$$

This dimensionless conductivity allows us to determine the skin factor of the rock at the fracture site. Table 2 shows the average permeability of the *I*, *H* and *G* horizons [13].

***Table 2**: The average permeability of the I, H and G horizons (Perenco-Rep/RDC).*

Horizons	Average permeabilities (mD)	Ratings
I	8.8	Average
H	16.8	Good
G	7	Average

- ✓ **Skin effect S_f** [23]**:**

$$Sf = -\ln\left(\frac{X_f}{r_w}\right) \quad (4)$$

With r_w: equivalent well radius, in ft;

- ✓ **Productivity growth J/Jo:**

$$\frac{J}{J_o} = \frac{\ln(\frac{r_d}{r_w})}{\ln(\frac{r_d}{r_w})+sf} \quad (5)$$

With: *J* - productivity index of the reservoir whose rock around the well has been fractured ((stb/D)/psi)

J_0 - productivity index for the reservoir where the rock around the well has not been fractured ((stb/D)/psi)

r_w – equivalent well radius

r_w and Sf are relatively well known, it remains to determine the drainage radius r_d (in ft) [22]

$$r_d = \sqrt{\frac{k*t}{377*\emptyset*\mu*C_t}} \quad (6)$$

With:

- ∅: average porosity of the Cenomanian reservoir (%);
- μ: viscosity of the oil (cp) ;
- C_t: total compressibility of the Cenomanian reservoir is the inverse of pressure unit (1/psi)
- *k*: average permeability of the Cenomanian reservoir (mD);
- *t*: production time at constant flow rate (s);

Where ∅, μ, C_t and *k* are respectively:

- Horizon *I*: 14.6%, 3.96 cp, $2.64*10^{-4}$ and 8.8 mD
- Horizon *H*: 15.4%, 3.96 cp, $2.64*10^{-4}$ and 16.8 mD
- Horizon *G*: 14.5%, 3.96 cp, $2.64*10^{-4}$ and 7 mD

The production time is not given because the driller did not carry out pumping tests in well MS-09. We therefore make a comparison with well MS-01 to estimate the test time. In well MS-01, the operator carried out production tests with a flow rate of 50bbl/d [12]. By analogy, we take a time of 24 hours to determine the drainage radius in well MS-09.

- **Tracing the Inflow Performance Relationship (IPR)**

Knowing the productivity growth, we can determine the productivity indices before and after fracturing. [26, 27]

IP before fracturing (J_0)

The basic formula for single-phase radial pseudo-permanent flow to a complete vertical well and when the reservoir pressure (P_r) is known allows us to determine the reservoir IP before fracturing [23]

$$J_o = \frac{Q}{\bar{P} - P_{wf}} = \frac{k \times h}{141.2 \times B_o \times \mu_o \left[\ln\left(\frac{r_d}{r_w}\right) - \frac{3}{4} + S\right]} \quad (7)$$

Post-fracking PI (J)

Knowing the productivity growth and the IP before fracturing, we can derive the IP after fracturing.

IPR for two-phase flow

The IPR curve for a two-phase radial flow is a graph obtained by plotting the pressure at the bottom of the well (pwf) on the ordinate and the flow rate produced (Q) on the abscissa.

Pressure is related to flow by the Vogel formula below [27]:

$$\frac{Q_o}{Q_{omax}} = 1 - 0.2\left(\frac{P_{wf}}{\bar{P}}\right) - 0.8\left(\frac{P_{wf}}{\bar{P}}\right)^2 \quad (8)$$

with:

P_{wf}: pressure at the bottom of the well in psi

$\bar{P}$: Average reservoir pressure, in psi

Q_0: flow rate produced before fracturing, in cubic feet per second

Q_{omax}: maximum flow rate reached before fracturing; Q_{omax} can theoretically be estimated using the average pressure $\bar{P}$ and the productivity index for a monophasic flow when the pressure is above the bubble point by the following equation: [24]

$$Q_{omax} = \frac{J_o * \bar{P}}{1.8} \quad (9)$$

After hydraulic fracturing, Vogel's formula can be written [24]:

$$\frac{Q}{Q_{max}} = 1 - 0.2\left(\frac{P_{wf}}{\bar{P}}\right) - 0.8\left(\frac{P_{wf}}{\bar{P}}\right)^2 \quad (10)$$

with:

Q: flow rate produced after fracturing, in cubic feet per second

Q_{max}: maximum flow rate reached after fracturing, in cubic feet per second,

and by analogy, we will have:

$$Q_{max} = \frac{J * \bar{P}}{1.8} \quad (11)$$

The variation in flow rate as a function of the pressure at the bottom of the well can therefore be followed, as shown in equation (11) below:

$$Q_o = Q_{omax}\left(1 - 0.2\left(\frac{P_{wf}}{\bar{P}}\right) - 0.8\left(\frac{P_{wf}}{\bar{P}}\right)^2\right) \quad (12)$$

RESULTS

For a better analysis of the fracture geometry, we produce graphs that allow us to follow the evolution of these parameters in relation to each other. These graphs are produced using Grapher software, which offers a better rendering of the curves best suited to our study, with greater precision in interpreting the data.

- **2D graphical analysis with two parameters**

Grapher software enabled us to observe the evolution of the depth parameter in relation to the others. Figures 2, 3, 4 and 5 show respectively:

Figure 2 - The variation in fracture width in relation to depth;

Figure 3 - variation in length as a function of depth;

Figure 4 - conductivity as a function of depth;

Figure 5 - the number of perforations as a function of depth.

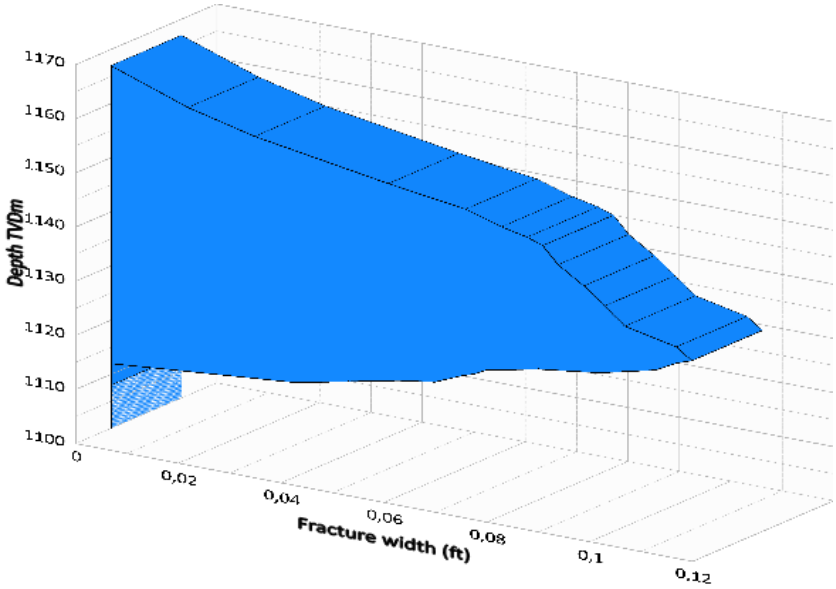

***Figure 2**. The variation in fracture width in relation to depth*

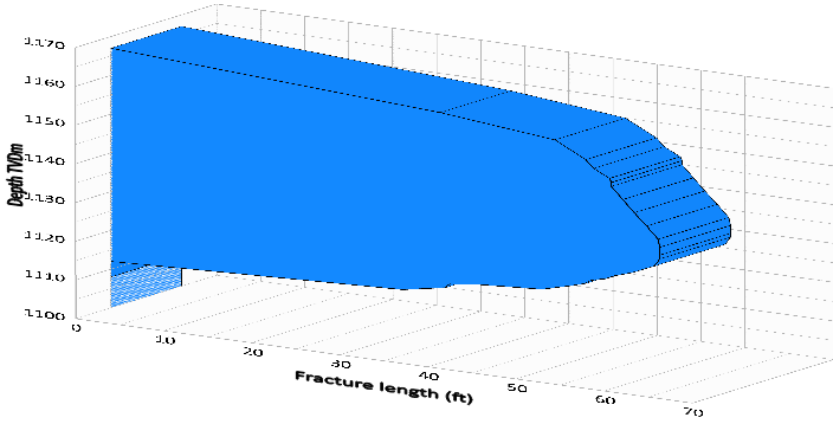

***Figure 3**. Variation in length as a function of depth*

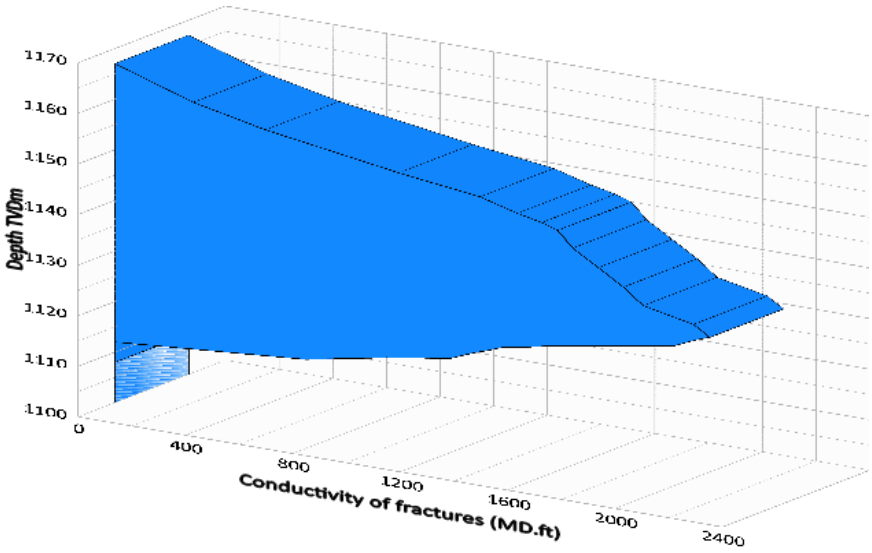

***Figure 4**. Conductivity as a function of depth.*

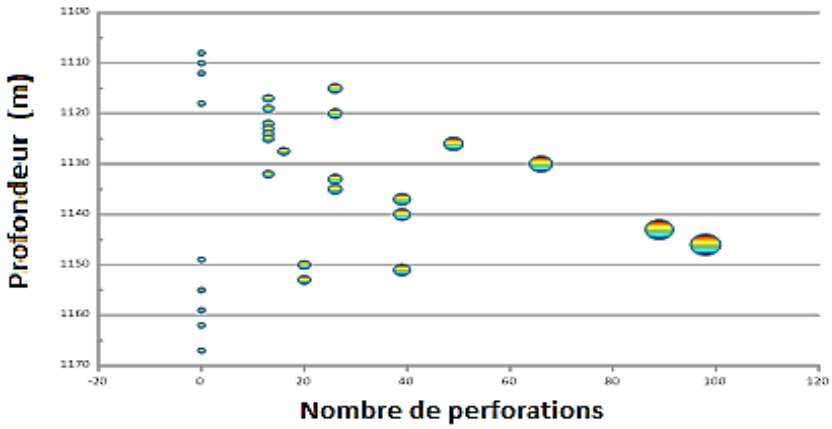

***Figure 5**. Number of perforations as a function of depth*

The figures show that the results converge at every depth level:

- Between the depths of 1108 and 1112m, since there has been no perforation or fracturing, the width, length and conductivity are zero (Figures 2, 3, 4 and 5);
- From 1115m, there is the first perforation and the first fracturing, which means that the width, length and conductivity are low (Figures 2, 3, 4 and 5);
- From 1115m, the curves follow an increasing trend until they reach a depth of 1133m, where the curves reach their maximum values, i.e. 0.113ft (figure 2) for width, 62.3 (figure 3) for length and 22.16 (figure 4) for conductivity. It should be noted that at this depth, the number of perforations had not reached the maximum peak, i.e. 26. The maximum peak in the number of perforations is 98, reached at a depth of 1146.
- Beyond 1133m, the curve decreases until it reaches zero at the wall, i.e. 1167m. Only the perforation curve stops at 1155m (Figures 2,3,4 and 5);

- **2D graphic analysis with three parameters**

Here we draw a graph in the form of a map in which two axes represent two parameters and we follow the evolution of a third parameter in relation to the first two. Figures 6, 7, and 8 show respectively:

Figure 6 - The evolution of width in relation to both length and depth

Figure 7 - Changes in conductivity as a simultaneous function of length and depth

Figure 8 - The distribution of proppants in relation to length and depth

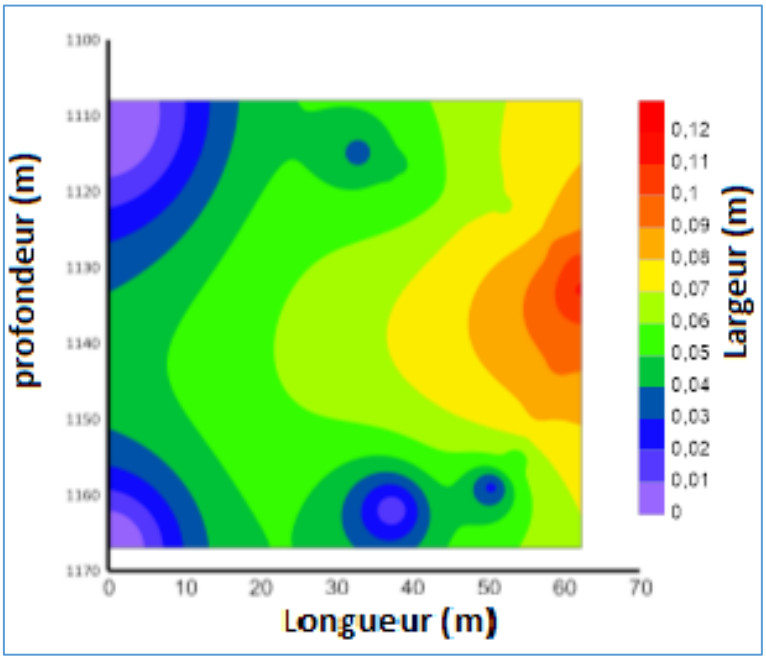

***Figure 1**. The evolution of width in relation to both length and depth*

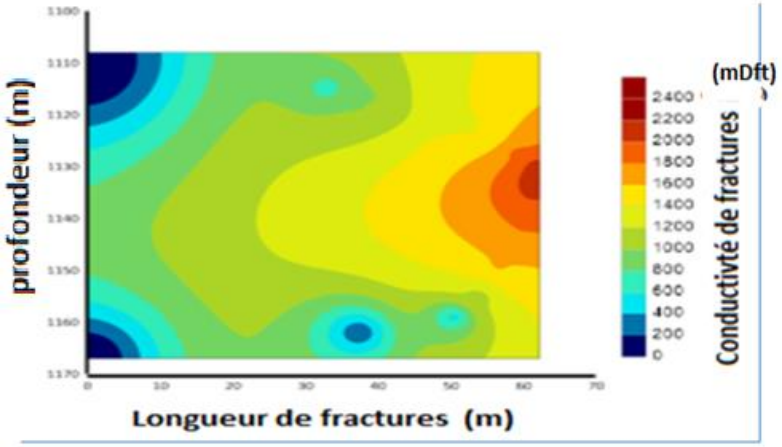

***Figure 2**. Changes in conductivity as a simultaneous function of length and depth.*

In Figure 7, we see that depths with long fractures also have high conductivity. And in depths with short fracture lengths, conductivity is also low.

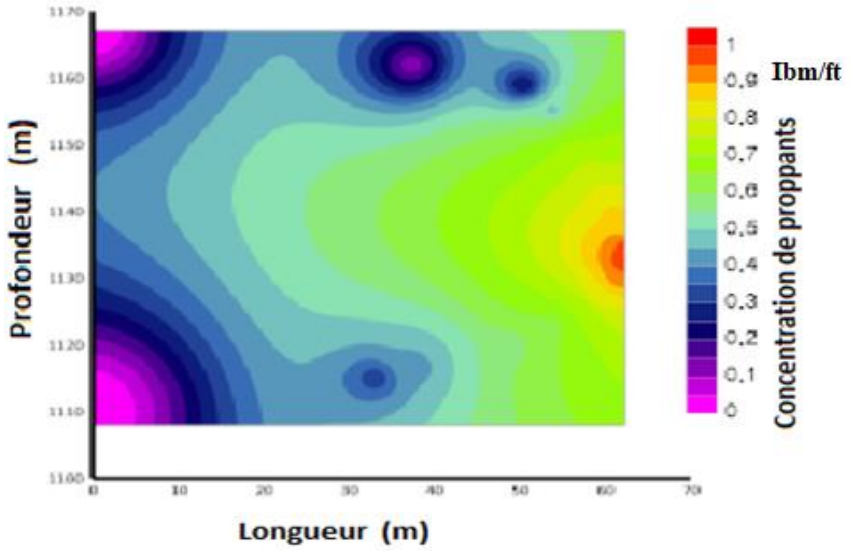

Figure 8. *The distribution of proppants in relation to length and depth.*

The figure 8 shows the distribution of proppants in the fractures. Each fracture contains a precise number of proppants; the distribution of these proppants in relation to each depth therefore depends on the length of the fractures. [25] The greater the length, the greater the concentration of proppants. The depth at which this concentration is highest is between 1133m and 1140m.

- **3D graphical analysis with four variables**

We have a 3D system represented by three axes and a variable independent of these three directions. It is the evolution of the third variable that interests us here, so we study it through the following graphs. Figure 9 shows the variables: depth, width, number of perforations and length.

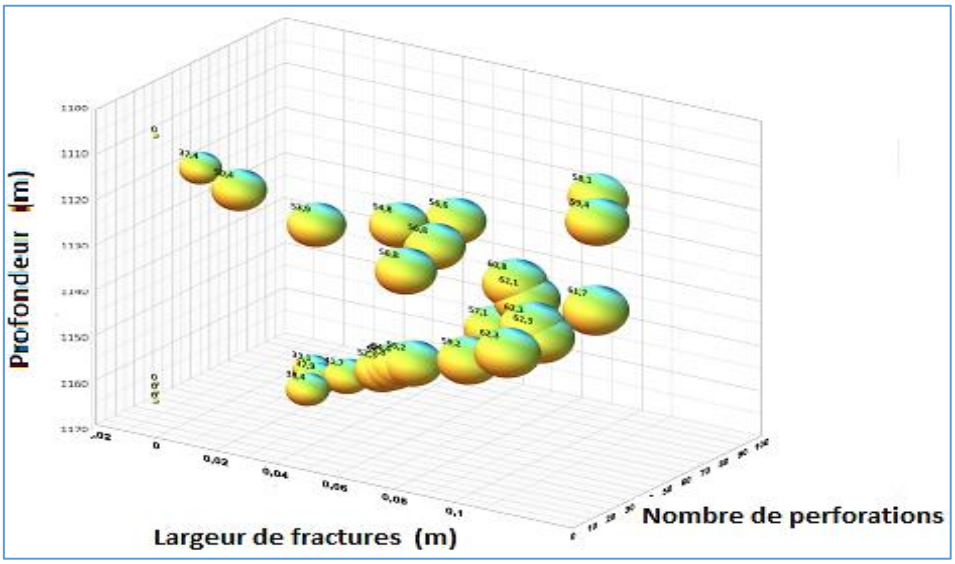

Figure 9. *Graphic 3D: depth, width, number of perforations and length*

The grain size and the number on each grain represent the evolution of the length in relation to each axis.

We can thus identify three zones that show the evolution of length in relation to each axis:

- Zone *a*: For a depth between 1108 and 1167m, a width between 0 and 0.046ft, a perforation between 50 and 98 holes; the maximum length reached is 56.8ft.
- Zone *b*: For a depth between 1118 and 1155m, a width between 0.051 and 0.078ft, a perforation between 0 and 39 holes; the maximum length reached is 56.6ft
- Zone *c*: For a depth between 1126 and 1150m, a width between 0.081 and 0.113ft, a perforation between 0 and 39 holes; the maximum length reached is 62.3ft.

In this way, we can see the evolution of the length in relation to each level of depth, the width and also the number of perforations.

Similarly, Figure 10 shows the grain size and the number on each grain represent the evolution of the width in relation to each axis. We can thus identify three zones showing the evolution of the width in relation to each axis:

- Zone *a*: For a depth between 1108 and 1167m, a length between 0 and 48.9ft, a perforation between 0 and 26 holes; the maximum width reached is 0.063ft.
- Zone *b*: For a depth between 1122 and 1159m, a length between 50.4 and 59.2ft, a perforation between 0 and 98 holes; the maximum width reached is 0.095ft
- Zone *c*: For a depth between 1130 and 1143m, a length between 59.4 and 62.3ft, a perforation between 13 and 89 holes; the maximum width reached is 0.1113ft.

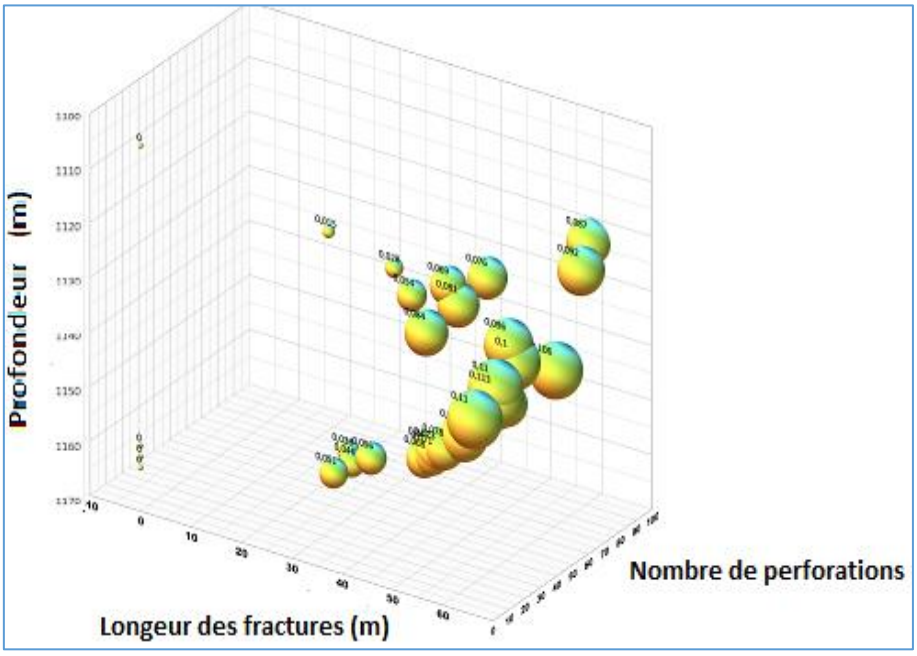

Figure 10. *Graph showing the evolution of width in relation to depth, length and number of perforation*

Thus, we can read the evolution of the width in relation to each level of depth, in relation to the length but also in relation to the number of perforations.

Operating as follows: Depth, length, width and conductivity, we obtain figure 11 below.

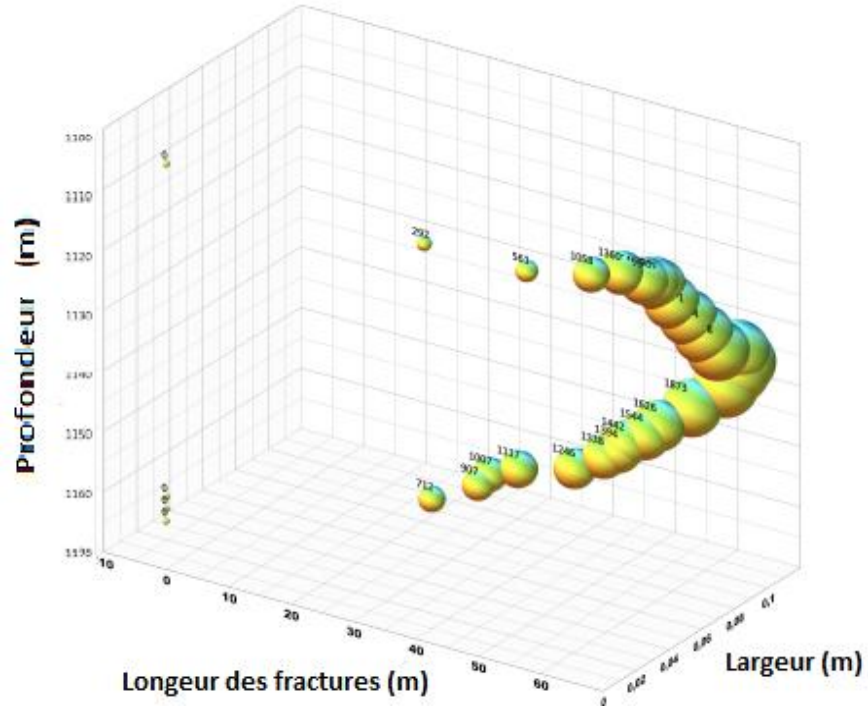

Figure 11. *Graph showing the evolution of conductivity with respect to depth, width and length*

The grain size and the number on each grain represent the evolution of conductivity in relation to each axis. We can thus identify three zones showing the evolution of conductivity in relation to each axis:

- Zone *a*: For a depth between 1108 and 1167m, a length between 0 and 37.9ft, a width between 0 and 0.046 holes; the maximum conductivity reached is 907MDft.
- Zone *b*: For a depth between 1118 and 1155m, a length between 38.4 and 56.2ft, a width between 0.051 and 0.078 holes ; the maximum conductivity reached is 1544 MDft
- Zone *c*: For a depth between 1126 and 1150m, a length between 56.6 and 62.3ft, a width between 0.081 and 0.113 holes; the maximum conductivity reached is 2216 MDft

In this way, we can see the change in conductivity at each depth level, in relation to length and also width.

- **Calculating productivity growth and plotting IPR for each horizon**

In order to better present our results for constructing the IPR for each horizon (I, G and H), we present the elements in Table 3 below:

***Table 3**: Summary of calculated productivity parameters for each horizon*

Horizon	x_f (ft)	Kf *(mD)*	F_{CD}	Sf	r_d	$\frac{J}{J_o}$	J_o	J
I	9.12	19744.36	5.46	−2.77	60.58	2.02	0.0315	0.0634
H	26.33	19735.85	3.23	−3.62	80,53	2,68	0.0567	0.152
G	28.32	19655.72	7.25	−3.99	54.22	3,88	0.0863	0.335

At Horizon I, fracturing increased reservoir productivity by a factor of 2.02. This means that the same bottom pressure (pwf) produces at a rate 2.02 times greater after fracturing than before fracturing. The IPR of a reservoir is a tool that enables the production engineer to determine the productivity of an oil reservoir. Here, we plot the Inflow Performance Relationship (IPR) before and after hydraulic fracturing to demonstrate the impact of hydraulic fracturing and therefore of fracture geometry on hydrocarbon drainage. Using equation 9, we obtain the flow rate produced before fracturing (Q_{omax}) which is 28.42 STB/D and and maximum flow rate reached after fracturing (Q_{max}), which is 57.26 STB/D. Table 4 below shows the variation in flow rate as a function of bottom pressure. This has enabled us to construct the IPR curve as shown in Figure 13.

***Table 4**: Flow rates as a function of downhole pressure before and after hydraulic fracturing in layer I*

Pwf	Q_o (before)	Q (after)
1625	0	0
1600	0.78170201	1.57494952
1400	6.64753065	13.3938478
1200	11.8250928	23.8248388
1000	16.3134885	32.8679225
800	20.1130177	40.5230989
600	23.2236804	46.7903679
400	25.6454766	51.6697296
200	27.3784064	55.1611839
100	27.9865463	56.3864459
50	28.2260351	56.8689605
0	28.4224697	57.264731

This graph shows the evolution of reservoir productivity before and after hydraulic fracturing in horizon I. We can see a very significant increase in reservoir productivity after fracturing, in line with the prediction made when productivity growth was calculated. This is reflected in the fact that the productivity curve after fracturing is more than double the productivity before fracturing.

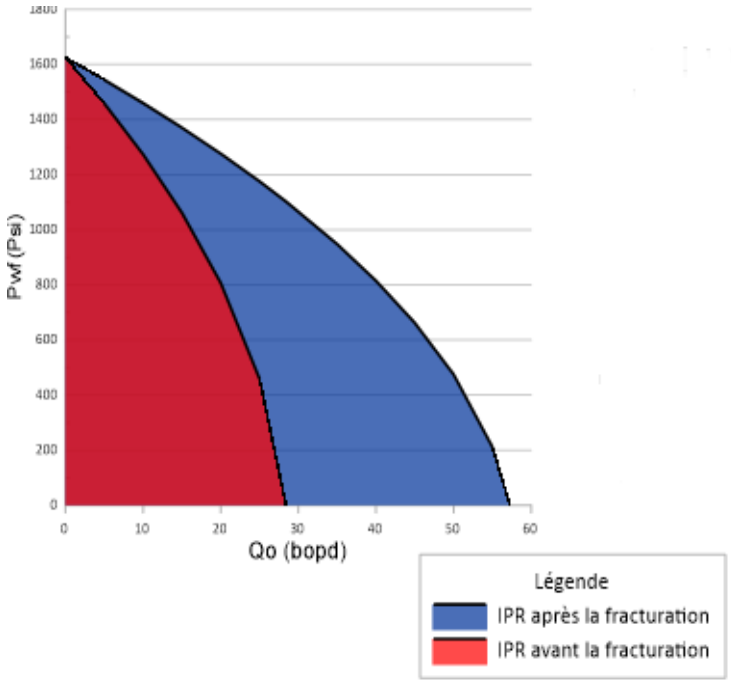

***Figure 13**. IPR before and after hydraulic fracturing in layer I in 2D*

In the H horizon, fracturing increased reservoir productivity by a factor of 2.68. This means that the same bottom pressure (P_{wf}) produces at a rate 2.68 times greater after fracturing than before fracturing. We have therefore drawn up Table 5 and Figure 14, based on the H layer below. With Q_{omax} = 51.19STB/D and Q_{max} = 137.07STB/D.

***Table 5**: Flow rates as a function of downhole pressure before and after hydraulic fracturing in the H*

Pwf	Q_o (before)	Q (after)
1625	0	0
1600	1.40781956	3.76986451
1400	11.972524	32.0600698
1200	21.2966026	57.0281225
1000	29.3800554	78.6740227
800	36.2228823	96.9977703
600	41.8250834	111.999365
400	46.307608	123.678808
200	49.307608	132.036098
100	50.402848	134.968936
50	50.8341593	136.123903
0	51.1879315	137.071235

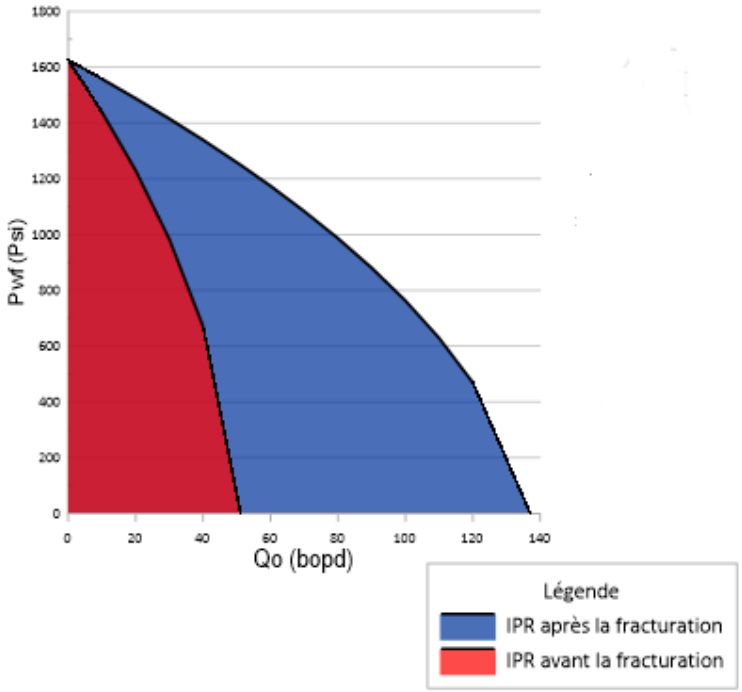

Figure 14. *IPR before and after hydraulic fracturing in the H layer*

This graph shows the evolution of reservoir productivity before and after hydraulic fracturing in the H horizon. We can therefore see a very significant increase in reservoir productivity after fracturing. This trend is in line with the prediction we made when calculating productivity growth. This is reflected in the fact that the productivity curve after fracturing is more than double the productivity before fracturing. Example: for a pressure of 1000psia, the flow rate increases from 29.38STB/D to 78.67STB/D after hydraulic fracturing. This shows the influence of fracturing geometry on the flow of hydrocarbons at the H horizon.

As for the G horizon, fracturing increased reservoir productivity by a factor of 3.88. This means that the same bottom pressure (pwf) produces at a rate 3.88 times greater after fracturing than before fracturing. By analogy with the IPR curves plotted for the I and H horizons, we have: Q_o = 77.87 STB/D and Q_{max} = 302.06 STB/D. This gives us Table 6 below and Figure 15.

Table 6: *Flow rates as a function of downhole pressure before and after hydraulic fracturing in the G layer*

Pwf	**Q_o (before)**	**Q (after)**
1625	0	0
1600	2.14168039	8.30748079
1400	18.2134988	70.6493332
1200	32.3979844	125.670308
1000	44.6951372	173.370404
800	55.1049572	213.749622
600	63.6274444	246.807962

400	70.2625987	272.545424
200	75.0104203	290.962008
100	76.6765813	297.424971
50	77.3327244	299.97012
0	77.8709091	302.057714

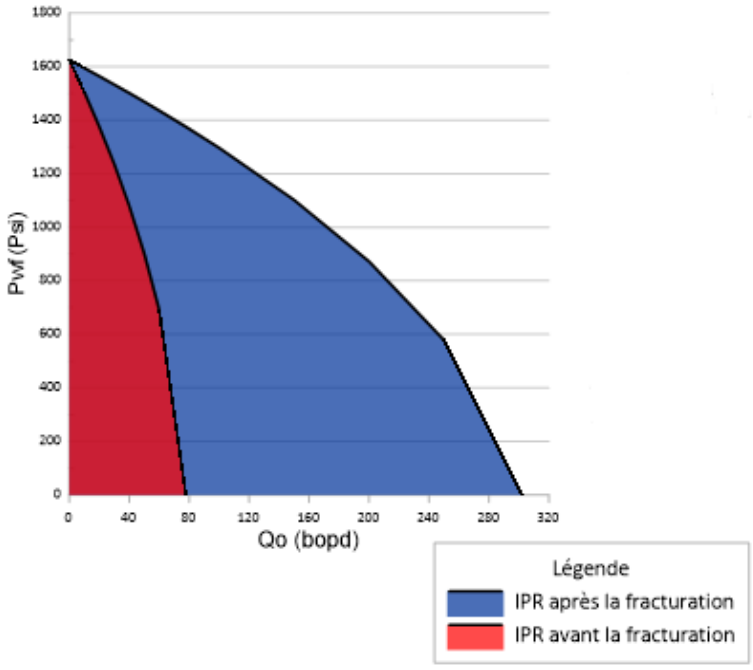

***Figure 16**. IPR before and after hydraulic fracturing in the G layer.*

This graph shows the evolution of reservoir productivity before and after hydraulic fracturing in the G layer. There is a very significant increase in reservoir productivity after fracturing. This trend is in line with the prediction we made when calculating productivity growth. This is reflected in the fact that the productivity curve after fracturing is three times that before fracturing.

CONCLUSION

In closing, a good knowledge of fracture geometry makes it possible to predict the nature and type of flow in the reservoir. Thus, we have provided the impact of hydraulic fracturing on low-permeability reservoirs and those whose permeability has been damaged by drilling operations.

The Cenomanian reservoir in the Makelekese field has a faulted anticlinal structure reflecting the tectonic and structural evolution of the environment. The mean oil thickness of the Cenomanian is around 100m, with a gas dome boundary averaging 25m. The oil-gas contact is observed in zones J and K, and the oil-water contact between zones G and F.

The IPR curves show the direct contribution of this geometry to productivity in the Cenomanian reservoir. For the three horizons in which fracturing was carried out, we noted an improvement in productivity of at least twice that seen before fracturing.

However, we noticed that for the same pressure at the bottom of the well, the flow rate at least doubled for each fractured horizon. For the G horizon, the flow rate almost quadrupled, which is an exceptional result for the operator.

REFERENCES

[1] Barrau N., Introduction to hydraulic fracturing, concepts and definition, Technical Report EISTI, Pau, France, pp 7, 2016;

[2] Tshiband Diemu B., Cours de géologie du pétrole de la RDC; Université de Kinshasa. 2021

[3] André E., Comportement hydromécanique d'un réseau de fractures dans une formation granitique: Expériences de l'échelle centimétrique en laboratoire, à l'échelle métrique dans la carrière du Mayet de Montage. Thèse de doctorat en Géophysique interne, Institut de physique du globe (Paris). 2004.

[4] Belghoul A., Caractérisation pétrophysique et hydrodynamique du socle cristallin. Thèse Université de Montpellier II. P.267, 2007

[5] Perrodon A., Géodynamique gisement pétrolifères. Pétrole-géologie. Editeur: Masson. Paris, New York, Barcelone, Milan. Elf Aquitaine. Paris, Pau, Boussens 2e édition révisée et complétée. 1985

[6] Wetshondo Osomba D., Cours d'évaluation et calcul des réserves pétrolières, Université de Kinshasa, 2021

[7] Cossé R., Techniques d'exploitation pétrolière; Le gisement. Ed. Technip, IFP, Paris France, p.329, 1988

[8] Tshiband Diemu B., Cours de forage, Université de Kinshasa. 2021

[9] Tshiband Diemu B., Cours de gestion des operations de forage, Université de Kinshasa, 2021

[10] Lucia F.J., Carbonate reservoir characterization. The University of Austin, Bureau of economic geology, geological circular, P 342. 2007

[11] Perenco-REP (2018): Makelekese field story, Democratic Republic of Congo, pp 4, unpublished report

[12] General Secretariat of Hydrocarbons: The sedimentary basins of the DRC, unpublished, Democratic Republic of Congo pp 13, unpublished report

[13] Perenco-REP (2007): Geological well report MS-09, Democratic Republic of Congo pp 5, unpublished report

[14] Li S., Zhang D., Li X., A New Approach to the Modeling of Hydraulic-Fracturing Treatments in Naturally Fractured Reservoirs. SPE Journal, 22, 1064–1081, 2017

[15] Cheng L., Hydraulic fracturing: A practical guide for engineers and scientists. Gulf Professional Publishing, 2016

[16] King G.R., Hydraulic fracturing: A comprehensive review. Elsevier Science & Technology. 2010

[17] Al-Ameri, S., Al-Raheem, M.F., Fracture geometry and fluid flow in hydraulically fractured formations. Journal of Petroleum Science and Engineering, 142, 101-111. 2016

[18] Velasco S., Schapery R., Hydraulic fracturing: History, methods, and environmental impact. Springer Science & Business Media, 2009

[19] Kampata D., Cours de boues de forage; Université de Kinshasa. 2021

[20] Nguyen J., Techniques d'exploitation pétrolière, IFP, Ed. Technip Paris, p. 373, 1993

[21] Economides M.J., Nolte K.G., Reservoir stimulation, Wiley Publisher; 3e edition, p. 856, 2000

[22] Benhamida I., Lakhchakheche T., Saoudi A., Amélioration de l'injectivité de puits par fracturation hydraulique. Puits OMO473, mémoire master, Universite Kasdi Merbah Ouargla, Algeria, p.76, inédit. 2012

[23] Boubekri A., Mahamat H.S., Description of fracturing hydraulic technic conventionnelle and de Hiway fracturation, Academic Master's thesis; Algeria, 2012-2013

[24] Kasongo N., Hydrocarbon hydrogeology course, University of Kinshasa, unpublished, 2021

[25] Pana I., Ghetiu I.V., Stan I.G., Dinu F., Branoiu G., Suditu S., The Use of Hydraulic Fracturing in Stimulation of the Oil and Gas Wells in Romania. Sustainability. 14(9):5614. 2022

[26] https://wiki.pengtools.com/index.php?title=IPR

[27] Vogel J.V., Inflow Performance Relationships for Solution-Gas Drive Wells. Journal of Petroleum Technology. 20 (SPE-1476-PA). 1968

Received: May 2024; Revised: June 2024; Accepted: July 2024; Published: July 2024